Modelling of membrane bonding response
Part 2 finite element simulations of membrane adhesion tests

Liu, Xueyan; Kasbergen, Cor; Li, Jinlong; Scarpas, Tom; Tzimiris, Georgios

DOI
10.1080/10298436.2020.1763993

Publication date
2020

Document Version
Final published version

Published in
International Journal of Pavement Engineering

International Journal of Pavement Engineering

ISSN: 1029-8436 (Print) 1477-268X (Online) Journal homepage: https://www.tandfonline.com/loi/gpav20

Modelling of membrane bonding response: part 2 finite element simulations of membrane adhesion tests

Xueyan Liu, Cor Kasbergen, Jinlong Li, Tom Scarpas & Georgios Tzimiris

To cite this article: Xueyan Liu, Cor Kasbergen, Jinlong Li, Tom Scarpas & Georgios Tzimiris (2020): Modelling of membrane bonding response: part 2 finite element simulations of membrane adhesion tests, International Journal of Pavement Engineering, DOI: 10.1080/10298436.2020.1763993

To link to this article: https://doi.org/10.1080/10298436.2020.1763993

Published online: 18 May 2020.

INTERNATIONAL JOURNAL OF PAVEMENT ENGINEERING
https://doi.org/10.1080/10298436.2020.1763993

Taylor & Francis
Taylor & Francis Group

Modelling of membrane bonding response: part 2 finite element simulations of membrane adhesion tests

Xueyan Liu, Cor Kasbergen, Jinlong Li, Tom Scarpas and Georgios Tzimiris

Section of Pavement Engineering, Faculty of Civil Engineering & Geosciences, Delft University of Technology, Delft, Netherlands

ABSTRACT

The adhesive bonding strength of the membrane layers between the asphalt concrete surface layers and the decks of steel bridges has a strong influence on the fatigue life of orthotropic steel deck bridges (OSDBs). The interfacial properties between the membrane and the layers bonded to it have not been extensively studied in the current orthotropic steel deck bridge system. For the adequate characterisation of the adhesive-bonding strength of various membranes and surrounding materials on OSDBs and for the collection of the necessary parameters for finite element model, details of the membrane adhesion test (MAT) are introduced and simulated by using the adhesive traction-separation interface element which was developed in a companion paper to this contribution (Liu, X., Kasbergen, C., Li, J., & Scarpas, A. (2019). Modelling of membrane bonding response: part 1 development of an adhesive contact interface element. *International Journal of Pavement Engineering*). Parametric studies of the adhesive contact element utilised for modelling the membrane bonding layer in the MAT test have been performed on the basis of the combination of different critical strain energy release rates and the characteristic opening length in the constitutive model. Comparison of membrane deformation profiles and the in-time debonding force distribution between experimental observations and finite element simulations have been presented.

ARTICLE HISTORY
Received 23 May 2019
Accepted 27 April 2020

KEYWORDS
Adhesive bonding strength; contact interface element; membrane; asphalt concrete; orthotropic steel deck bridges; strain energy release rate; finite element

1. Introduction

A membrane in bridge surfacing systems is defined as a thin impermeable layer that is used in conjunction with asphalt wearing surface to protect the deck plate from the penetration of moisture. Most Canadian provinces and many European countries require the use of membranes on new bridge decks. About 60% of the U.S. state agencies use them with greater usage on existing bridge decks than new bridges (Russell 2012).

In literature, several groups of membranes could be identified based on certain distinctions, such as membranes with or without inlays (reinforced), preformed membranes (produced in a factory) or in-place formed membranes (liquid applied membranes). Preformed membranes involve the application of a primer to the clean bridge deck to improve the adhesion of the membrane to the deck. Some preformed membranes include a self-adhesive backing on the membrane sheet. These sheets can be rolled into place and then bonded to the deck primer using a roller. Others are bonded to the deck by heating the membrane using either a hand torch or a machine.

A number of techniques have been developed to quantify the adhesive strength between the membrane and the associated substrate. Among others, the blister test, initially suggested by Dannenberg (1958) and discussed by Gent and Lewandowski (1987), is most commonly used. The test specimen in the blister test consists of a perforated substrate with a thin flexible bonded membrane. A fluid is injected at the interface, through the perforation; the fluid causes a progressive debonding of the membrane. However, blister tests have several drawbacks, including that the strain energy release rate increases as the blister radius increases and that membrane debondings become unstable. The bulged area is anomalous and unpredictable, especially when the substrate materials are harsh and porous (e.g. cement concrete or porous asphalt concrete). The test is vague about the physical or chemical effects of the pressurised liquid on the interface between the two bonded materials.

The shaft-loaded blister test (SLBT), first proposed by Williams, is an alternative to the pressurised blister test (Williams 1969). A machine-driven shaft is utilised to induce central loads and displacements on the membrane. Because of the slightly simpler setup and loading method, the SLBT has advantages over the traditional blister test and has received much attention in the past two decades. The main limitation of the SLBT is the stress singularity caused by its shaft point load. Different shaft cap shapes are employed to improve this weakness. The most common improvement is to use a spherically capped shaft or ball with a certain radius (Liao and Wan 2001, Xu et al. 2003).

The peel test is another commonly used method to quantify the adhesive strength of the membrane to the associated substrate. However, the peel test usually causes large permanent deformation at the loading point and makes the calculation of the energy release rate inaccurate. The majority of the mechanical energy supplied in peeling is dissipated or stored in the deformation of the test specimen, and relatively little energy actually contributes to the fracture process of the interface.

CONTACT Xueyan Liu x.liu@tudelft.nl

In order to adequately characterise the adhesive bonding strength of the various membranes to surrounding materials on OSDBs and collect the necessary parameters for FE modelling, a Membrane Adhesion Tester (MAT) has been developed (see Figure 1). On the basis of experimental data obtained from the MAT device, ranking of the bonding characteristics of different membrane products can be performed as well as the role of other influencing factors, such as the substrate type and test temperature can be investigated. Availability of the MAT results together with the large scale accelerated pavement tester will allow a better understanding of performance of membrane layers in the bridge multilayers surfacing systems allowing optimisation of maintenance activities on OSDBs.

In this paper, the MAT test are briefly introduced to characterise the adhesive characteristics of various membranes and surrounding materials. Furthermore, the FE model of the MAT test will be presented. The progressive membrane debonding process of the MAT test will be modelled by using the adhesive traction-separation interface element which was developed in the companion paper to this contribution (Liu et al. 2019). The critical strain energy release rate which was measured from MAT will be utilised for the FE simulations. Parametric studies of the adhesive contact element utilised for modelling the membrane bonding layer in the MAT test have been performed on the basis of the combination of different critical strain energy release rates and the characteristic opening length in the constitutive model. A viscoelastic Zener model is utilised to simulate the viscoelastic response of the membrane materials in the MAT test. Comparison of membrane deformation profiles and the in-time debonding force distribution between experimental observations and finite element simulations have been drawn.

2. MAT set up

The MAT test system consists of a loading device, an environmental chamber, a laser-scanning device, and a data acquisition system. The loading device includes a computer-controlled loading component that, during each loading cycle in response to commands from the data-processing and control component, adjusts and applies a load on the tested membrane. The loading device is capable of (a) providing repeated haversine loading at a frequency range of 0–12 Hz, (b) lifting the piston to the maximum height of 130 mm after the piston comes into contact with the test membrane, (c) providing a maximum force of 2 kN, and (d) providing two piston heads with radii of 90 and 75 mm. Figure 2 illustrates the components of the MAT device.

The laser-scanning system senses the shape of the deformed object and collects data that define the location of the outer surface of the membrane. A line laser is utilised to measure the profile of membrane deformation over time across a 150-mm width. The laser scanner can be operated in a temperature range of −10°C to 55°C. The frequency of the laser scanner is up to 250 Hz for the full range.

An environmental chamber is utilised to enclose the entire test setup and maintain the specimen at a controlled temperature. The environmental chamber is not required if the temperature of the surrounding environment can be maintained within the specified limits. The chamber can provide a temperature range of −15°C to 80°C and a relative humidity range of 10–95%.

During each load cycle, the control and data acquisition systems can measure the load and deformation of the piston and adjust the load or displacement applied by the loading device and the loading frequency. In addition, the device can record load cycles, applied loads, and piston deformations.

3. FE modelling of membrane adhesion tests

3.1 FE model description

The membrane specimen is comprised of two parts, the membrane and the substrate. Details are described in Section 2. In the MAT tests, the specimen is fixed on the apparatus and then the membrane deforms with the elevation of the piston in the middle. The structural geometry of the MAT is shown in Figure 2.

The membrane is 400 mm in length and 100 mm in width. The thickness of the membrane differs according to the type of the membrane product. In order to have smooth contact to the

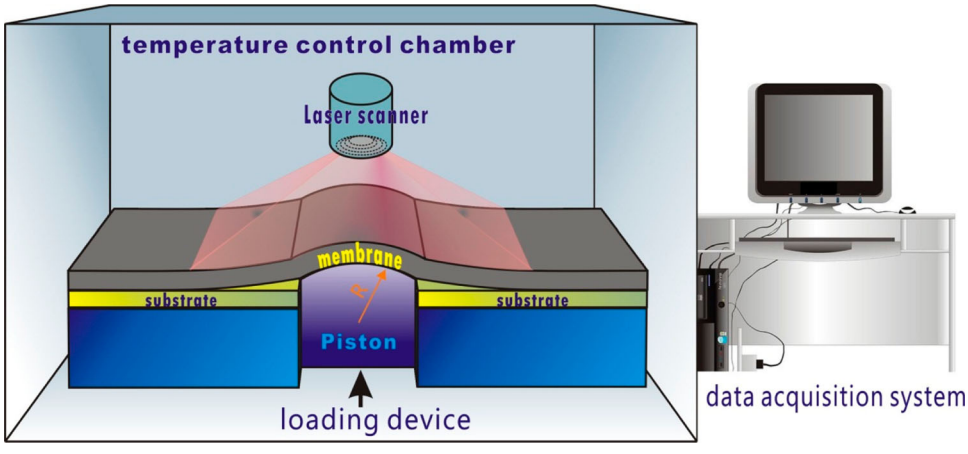

Figure 1. Schematic of the Membrane Adhesion Test (MAT) device.

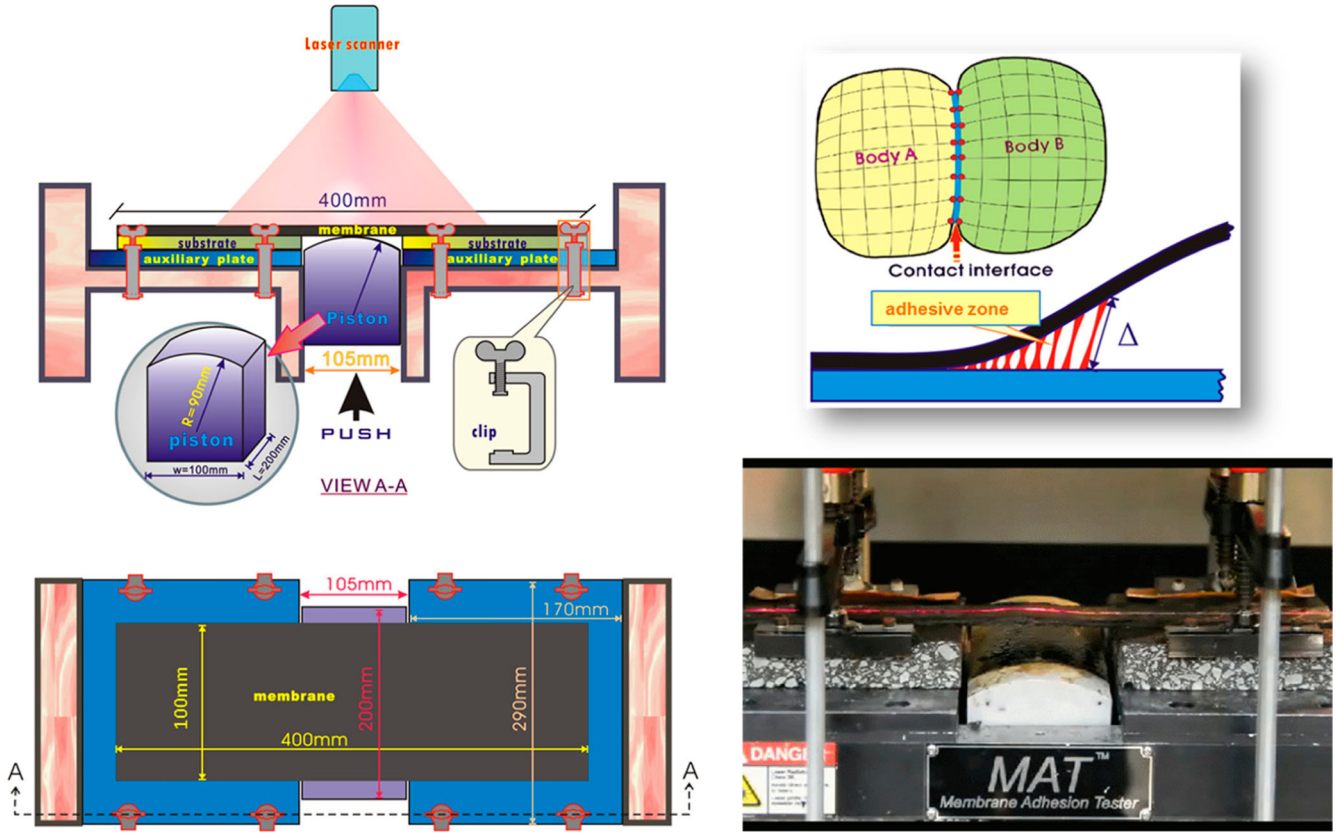

Figure 2. Set-up for MAT and element used for modelling debonding process.

membrane, the upper surface of the piston has a cylindrical shape. The radius of the piston is 90 mm and the width is 100 mm.

The finite element mesh consists of 20-noded brick elements, Figure 3. The mesh consists of four components: the membrane layer, the substrate, the piston and the contact interface elements, which represents the adhesive interface layer between the membrane and the substrate as well as the gap between the piston and the membrane. Because of symmetry, only a quarter of the MAT device is simulated for computational efficiency.

The boundary conditions for the MAT simulation are shown in Figure 4. It can be observed that, at the left side boundary ($x = 0$), all nodes are fixed. At the central plane ($x = 152.5$ mm), they can move freely in the vertical direction. The bottom surface of the substrate is rigidly fixed to the MAT frame. For monotonic test simulations, a displacement controlled load with a speed of 5 mm/s is applied vertically on the bottom plane of the piston.

3.2 Parametric study of the adhesive contact element by MAT

In order to simulate the bonding characteristics of the membrane to the substrate, the adhesive contact interface developed in the companion paper (Liu et al. 2019) together with the traction-separation law is utilised. From the traction-separation law, we know that the strain energy release rate G and the characteristic opening length δ_C control the adhesive strength of the contact interface. In order to study the influence of

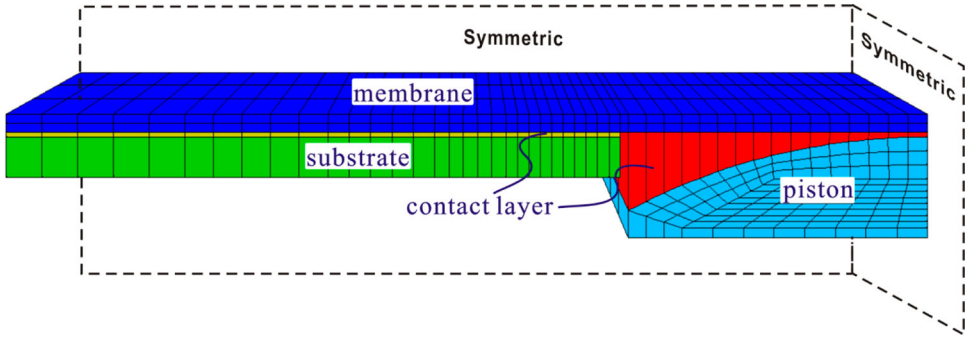

Figure 3. FE modelling for MAT simulation.

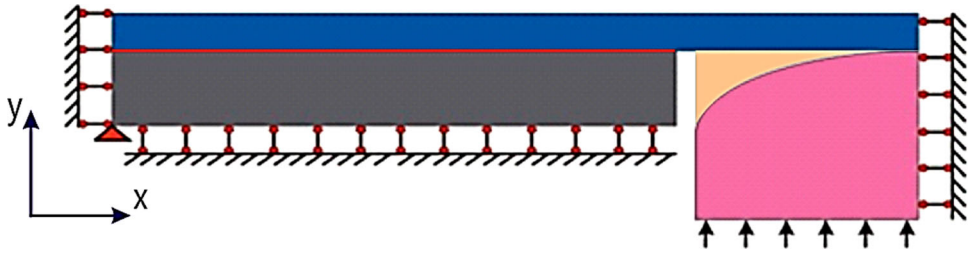

Figure 4. Boundary conditions for MAT FE simulations.

those two parameters on the simulation of the response of membrane debonding, two sets of simulations are carried out by varying those two parameters, respectively. In the numerical examples, the membrane is simply assumed as a linear-elastic material with Young's modulus 50 MPa and Poisson's ratio of 0.2. The membrane layer is adhered to a steel substrate plate with Young's modulus of 210,000 MPa and Poisson's ratio of 0.2. The membrane layers in the numerical examples are connected to the steel substrate by using the adhesive contact interface with appropriate constitutive parameters.

3.2.1 Influence of strain energy release rate G

According to the MAT tests (Liu et al., 2013), it was found that the range of the measured strain energy release rate for membrane bonded on the different substrates varies between 1 and 5 N/mm. In the following numerical examples, by fixing the model parameter $\delta_C = 2$ mm, the influence of strain energy release rate G values on the traction-separation response at the contact interface between membrane and steel substrate are illustrated in Figure 5. It can be observed that the parameter G can influence significantly the interaction between the membrane and the substrate. A higher G value results in a higher adhesive bonding strength of the contact interface, hence it leads to the higher debonding resistance of the membrane layer from the substrate. In the following numerical examples, the MAT tests were modelled by using the monotonic displacement controlled load applied from piston.

Figures 6 and 7 show that, at the same displacement controlled load, the membrane deforms both in vertical and horizontal directions. It can observed that, by assuming the different G values at the adhesive contact interface, the deformed membrane profiles are different. When the membrane layer bonded on the substrate with higher G value, it results to less debonding length propagation at the contact interface. Another observation is that membrane with higher G value can be stretched more at the part where there is no bonding to the substrate (i.e. above the piston head of MAT). This is due to the fact that, the membrane with higher G value leads to higher bonding strength at the bonding interface hence extra deformation has to be developed at the area without boundary constraint.

Figure 8 gives insight into the development of the damage at the interface between the membrane and the steel plate substrate after the piston has moved vertically to 40 mm. The damage value ranges from 0 to 1, which represents a membrane fully intact to fully debonded from its substrate. The figure shows that the damage in a membrane interface is highly related to its strain energy release rate G. A higher G value dramatically reduces or postpones the damage development at the adhesive interface layer.

Figure 9 shows the contour plot of interface damage at the last step of the MAT monotonic load simulation. It can be observed that, as the piston is moving up, damage starts from the bonding region, which is close to the piston and gradually develops to the rest of the bonded region. It can be also observed that both the opening and shearing deformations occur at the interface layer.

As it was mentioned above, in the numerical simulations, the membrane layers are subjected to a displacement-controlled load of 40 mm by the piston. This displacement-

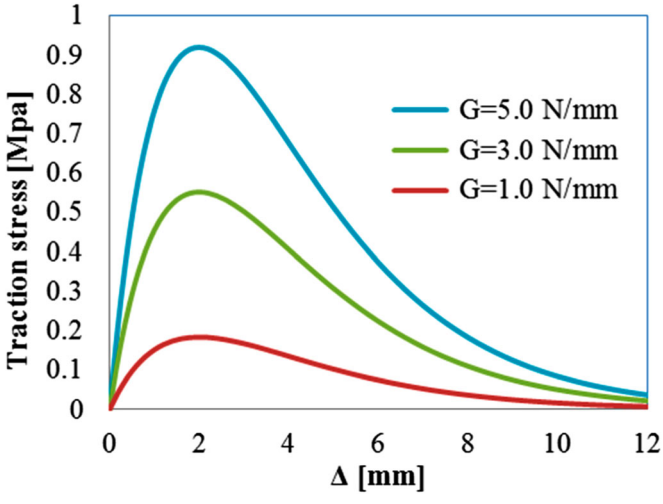

Figure 5. Traction-separation law (G = 1.0–5.0 N/mm, δ_C = 2.0 mm).

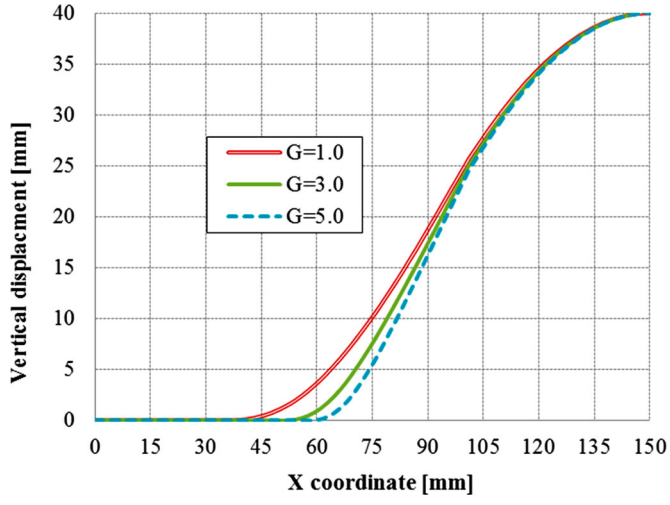

Figure 6. Membrane vertical displacements (G = 1.0–5.0 N/mm, δ_C = 2.0 mm, displacement control load at piston is 40 mm).

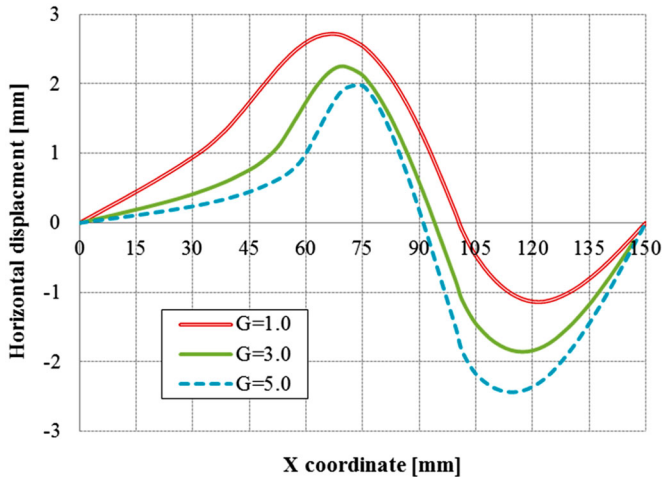

Figure 7. Membrane horizontal displacements (G = 1.0–5.0 N/mm, δ_C = 2.0 mm).

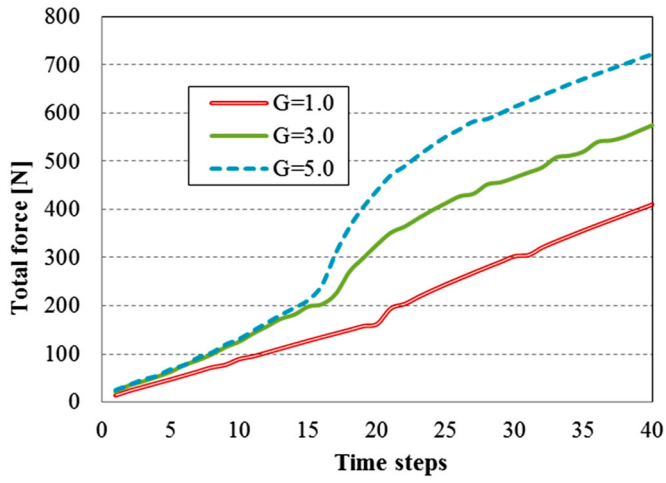

Figure 10. Simulated the piston reaction force (G = 1.0–5.0 N/mm, δ_C = 2.0 mm).

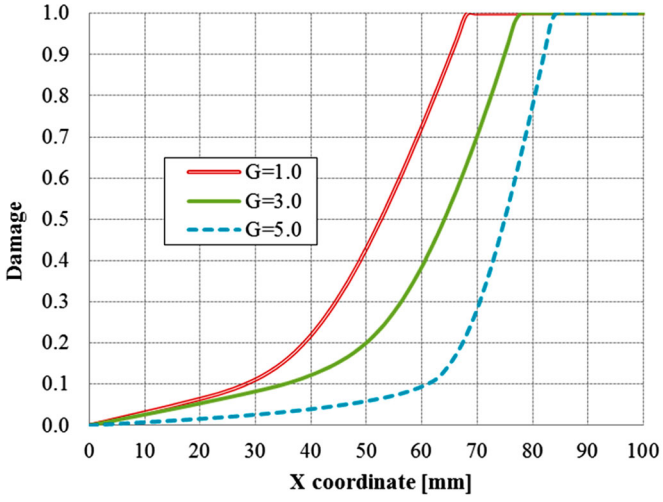

Figure 8. Interface damage (G = 1.0–5.0 N/mm, δ_C = 2.0 mm).

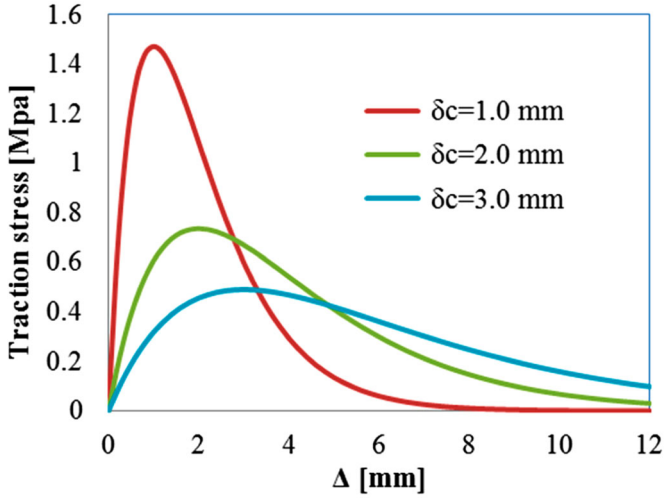

Figure 11. Traction-separation law (G = 4.0 N/mm, δ_C = 1.0–3.0 mm).

controlled load is applied linearly increasingly in 40 steps. The total reaction forces on the piston are plotted in Figure 10. It can be observed that the reaction force on the piston is increased by moving up the piston. The larger the interface G value is, the higher the reaction force that is generated on the piston. Due to symmetry, in the numerical examples, only a quarter of the MAT mesh was utilised for the simulations. Therefore, the real value of the reaction force on the piston

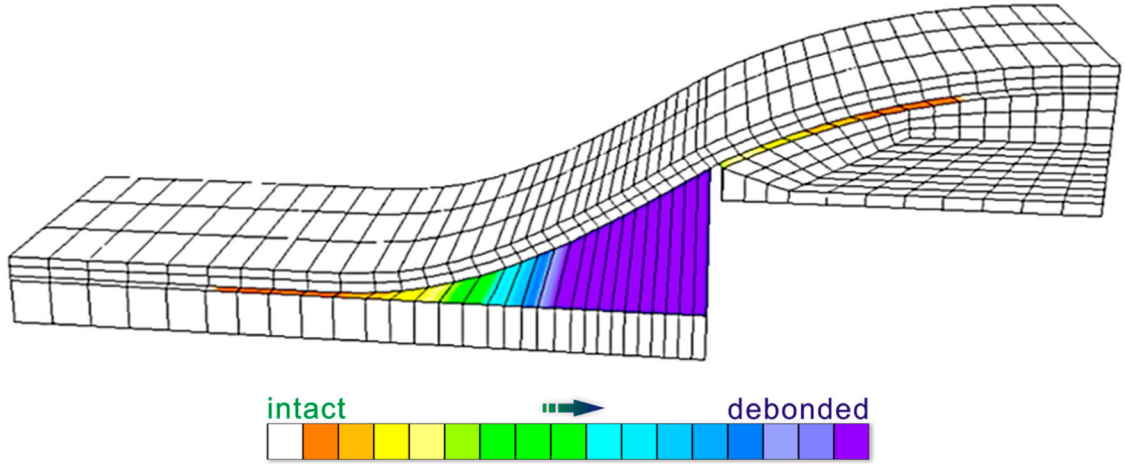

Figure 9. Interface damage distributions (G = 2.0 N/mm, δ_C = 2.0 mm, displacement control load at piston is 40 mm).

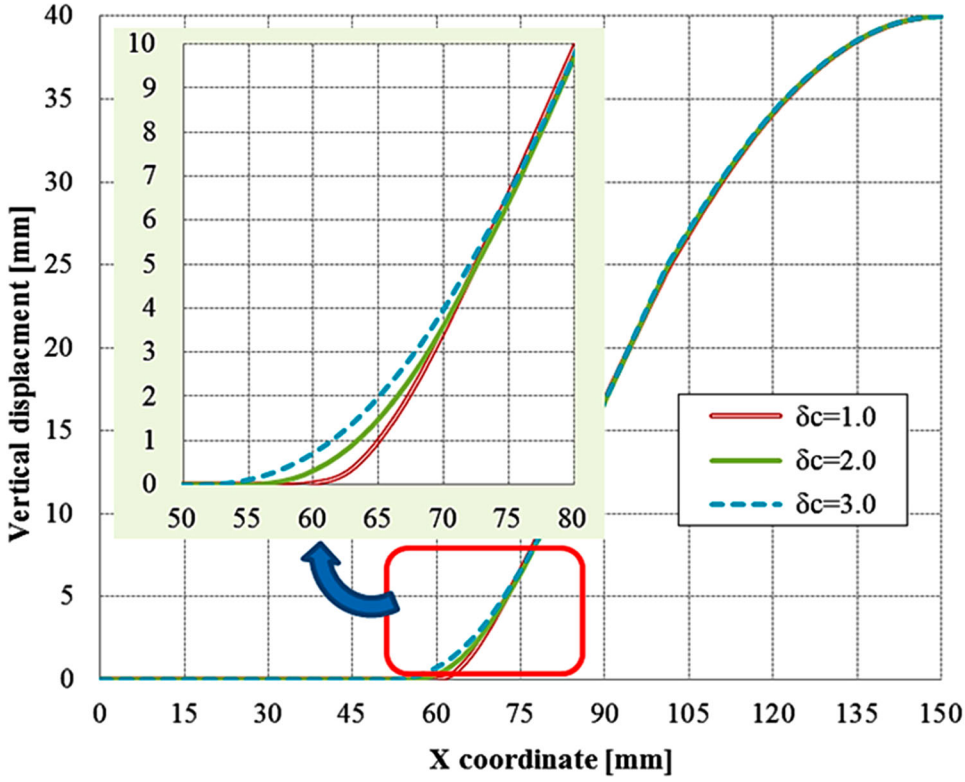

Figure 12. Membrane vertical displacements (G = 4.0 N/mm, δ_C = 1.0–3.0 mm).

should be multiplied by a factor four to the numerical results in order to obtain a comparison result with the MAT lab test. In later part of this paper, the FE simulations of real MAT tests for some membrane products will be discussed.

3.2.2 Influence of the characteristic opening length δc

In this section, the influence of the characteristic opening length δ_C in the adhesive traction-separation law of Equation (31) in the companion paper to this contribution (Liu et al. 2019) is studied by a series of FE simulations. In total three simulations are carried out by choosing δ_C values as 1.0, 2.0 and 3.0 mm. Throughout this set of simulations, the strain energy release rate G is fixed to 4.0 N/mm. Similarly to the examples used in the previous section, the MAT tests were modelled by using a monotonic displacement controlled load applied on the piston.

The plots of the adhesive traction-separation zone constitutive law with the predefined δ_C values are illustrated in Figure 11. It can be observed that, opposite to the effect of the parameter G, the higher δ_C value results in a lower adhesive bonding strength of the contact interface. Hence, it leads to a lesser debonding resistance of the membrane layer from the substrate.

Figures 12 and 13 show the membrane displacements in vertical and horizontal directions, respectively, for the five cases. Similarly to the cases with different G values in the previous

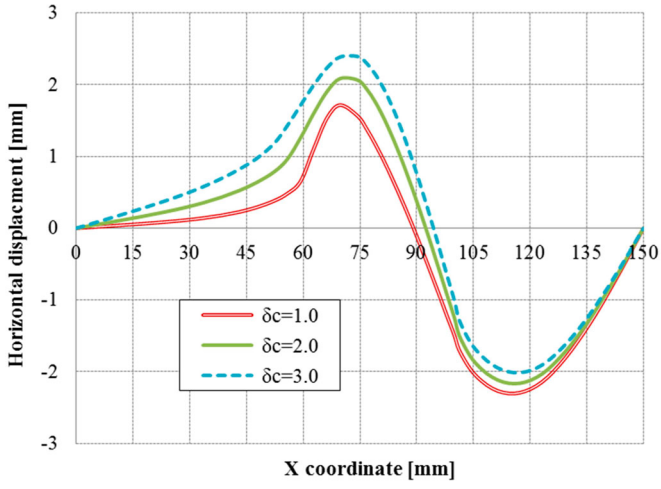

Figure 13. Membrane horizontal displacements (G = 4.0 N/mm, δ_C = 1.0–3.0 mm).

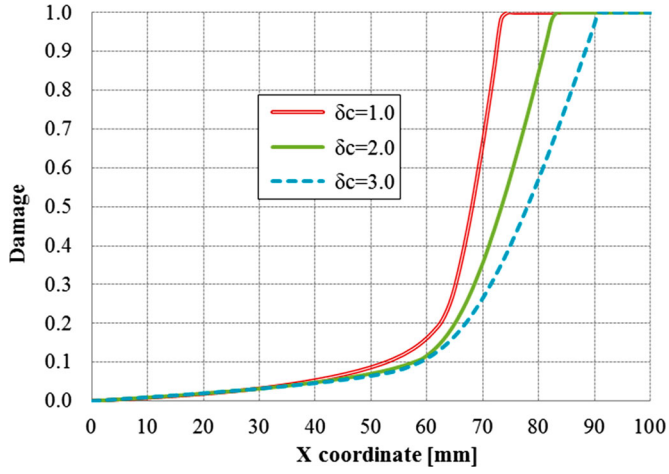

Figure 14. Interface damage (G = 4.0 N/mm, δ_C = 1.0–3.0 mm).

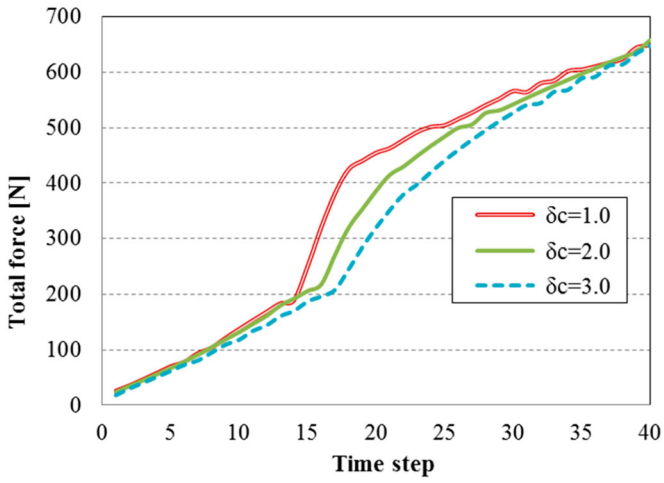

Figure 15. Piston total force (G = 4.0 N/mm, δ_C = 1.0–3.0 mm).

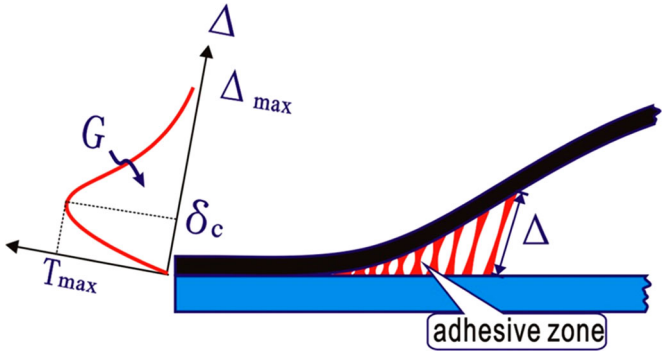

Figure 16. Schematic diagram of adhesive traction-separation model.

section, by specifying the different δ_C values at the adhesive contact interface, the deformed profiles of the membrane are different. However, opposite to the cases with different G, the membrane layer with higher δ_C value results to more debonding length propagation at the contact interface. The influence of δ_C is less obvious than that of the G value discussed in the previous section.

Figure 14 gives insight into the development of the damage at the interface between a membrane and its steel plate substrate after a piston vertical movement up to 40 mm. It can be observed that the damage in the membrane interface is highly related to its parameterδ_C. A higher δ_C value reduces damage development. This means that an interface layer with larger δ_c value is more ductile which could be also observed in Figure 11.

The influence of δ_C on the total reaction forces on the piston is plotted in Figure 15. It can be observed that the total reaction force on the piston is increased. The lower the value of δ_C is, the higher the piston total reaction force that is needed.

3.3 Finite element simulation of MAT

As mentioned before, the progressive membrane debonding process in a MAT test is modelled by the introduction of adhesive contact interface elements in the interface region between the membrane and the substrate.

As it is was also discussed in the companion paper to this contribution (Liu et al. 2019), for any given location along the adhesive interfacial zone, full membrane debonding occurs locally when the fibrils deform to a maximum allowable deformation limit of Δ_{max}, Figure 16. At that instant, as shown in Figure 16, the area under the traction – separation curve corresponds to the strain energy release rate G required for crack

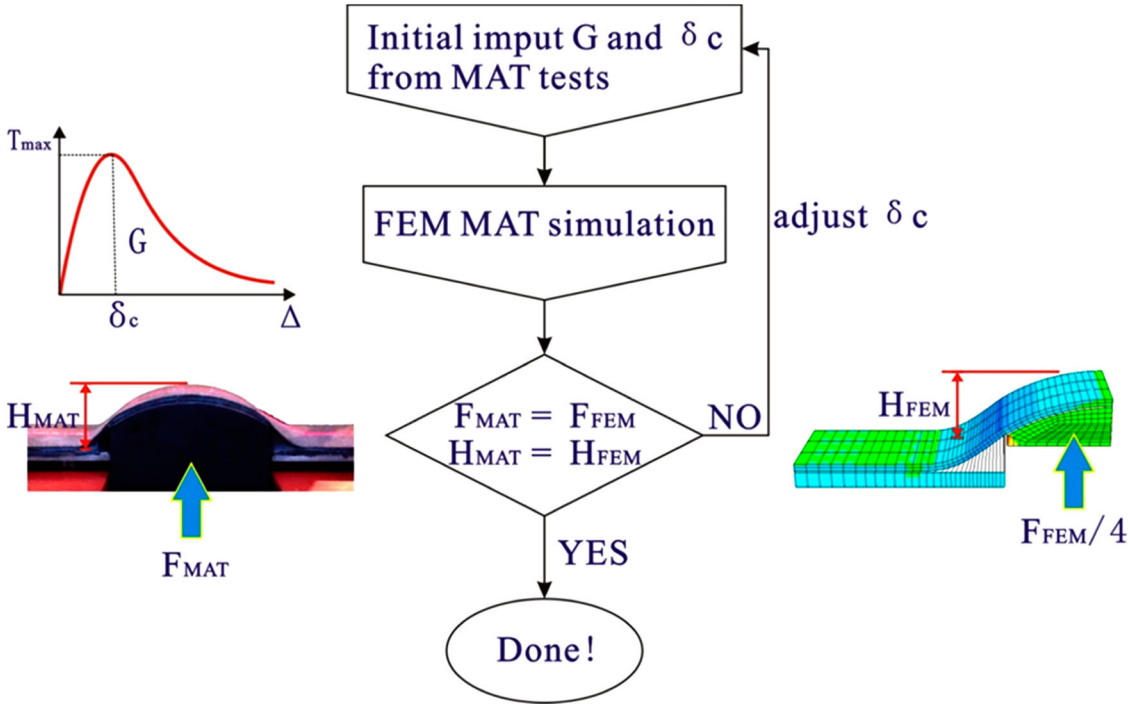

Figure 17. Iterative methodology for δ_c determination.

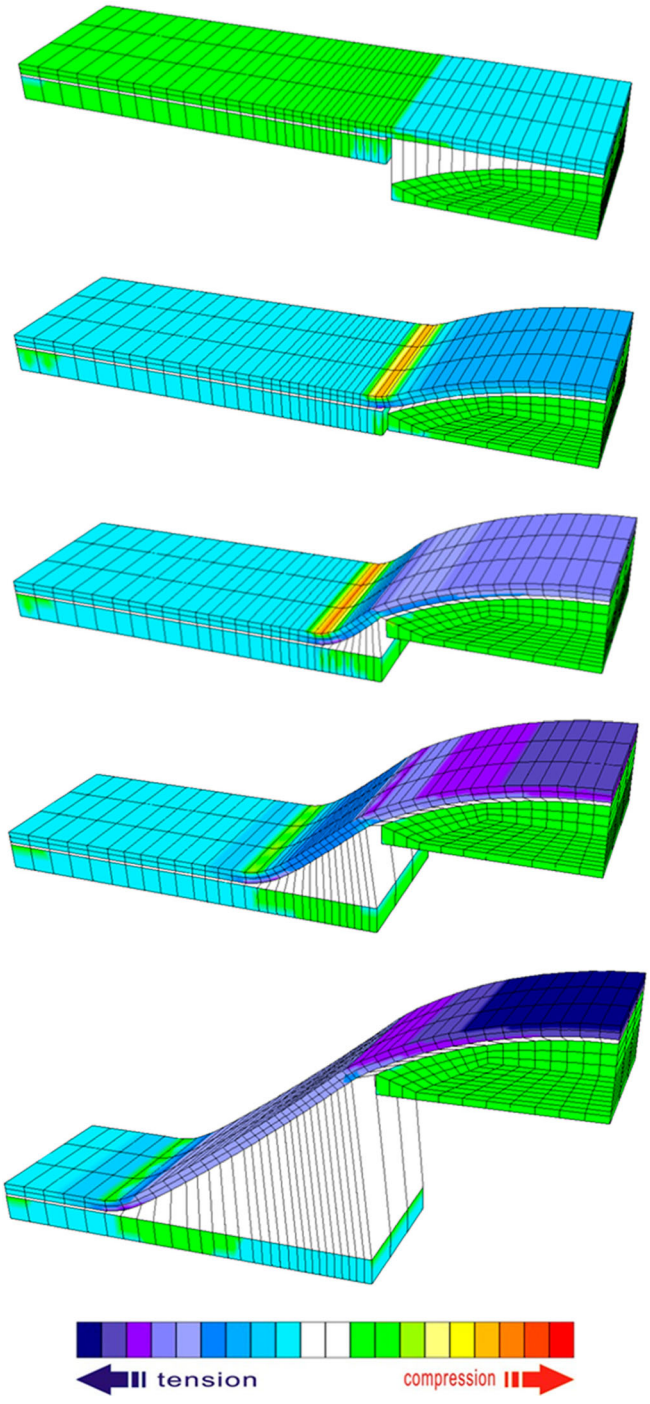

Figure 18. Evaluation of horizontal stress of MAT test, piston vertical displacement: 0, 10, 30, 50, 80 mm.

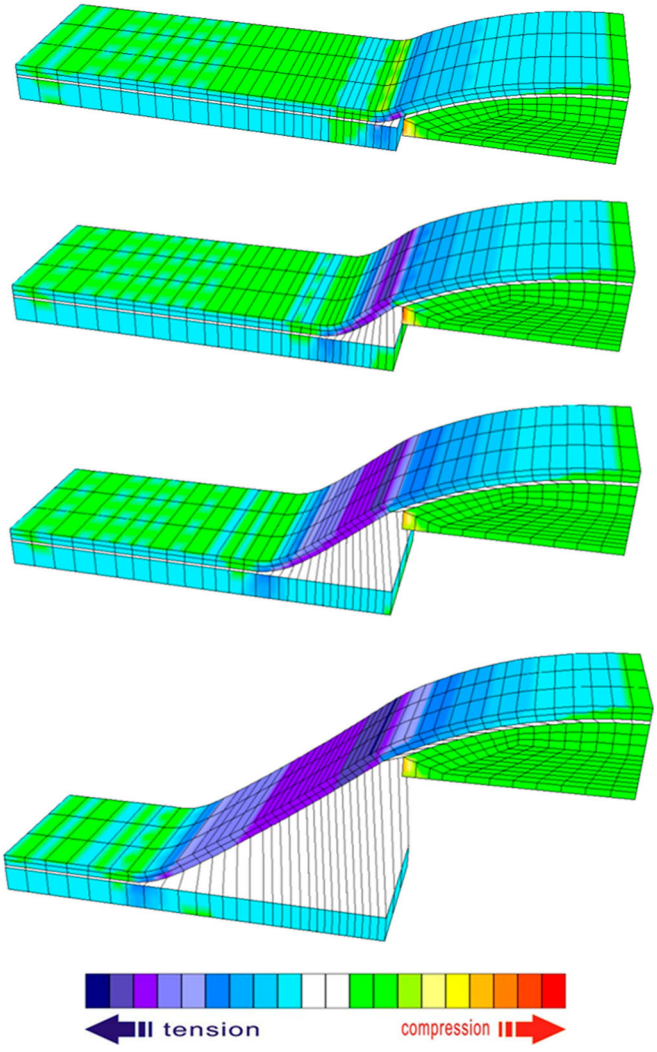

Figure 19. Evaluation of vertical stress of MAT test, piston vertical displacement: 10, 30, 50 and 80 mm.

extension. From the MAT tests in (Tzimiris 2017), for a given combination of membrane material and substrate, the parameter G can be measured. The other model parameter δ_C is difficult to obtain by experimental tests, and this parameter is quite effective since it controls the bonding stiffness as well as the adhesive strength $T_{\max}$. For this reason, an iterative approach with the FE method is developed to determine the δ_C value, Figure 17.

Using as an initial estimated measured value of δ_c, successive FE simulations are performed in which the finite element predicted overall deformation profile of the partially debonded membrane and the corresponding piston force are compared with the experimentally measured ones. As shown in Figure 17, this iterative process is repeated until satisfactory matching is obtained between the finite element results and the experimental ones.

Company A provided two membrane products for the MAT tests, which are called membrane A1 and A2. Membrane A1 and A2 are waterproof membranes manufactured with SBS elastomeric bitumen and internally reinforced with a non-woven polyester textile. Membrane A1 is used only at the bottom membrane layer in bridge. The membrane A1 specimen adhered to the steel deck and the Guss Asphalt (GA) are denoted as Steel/A1 and A1/Guss respectively.

Membrane A2 is used as the top membrane layer in the bridge. The membrane A2 specimen adhered to the Guss Asphalt (GA) is denoted as G-asphalt/A2; and the membrane A2 specimen connected to the Porous Asphalt (PA) is called A2/P-asphalt.

In the next section, numerical simulations of the response of membranes A1 in the MAT test are presented.

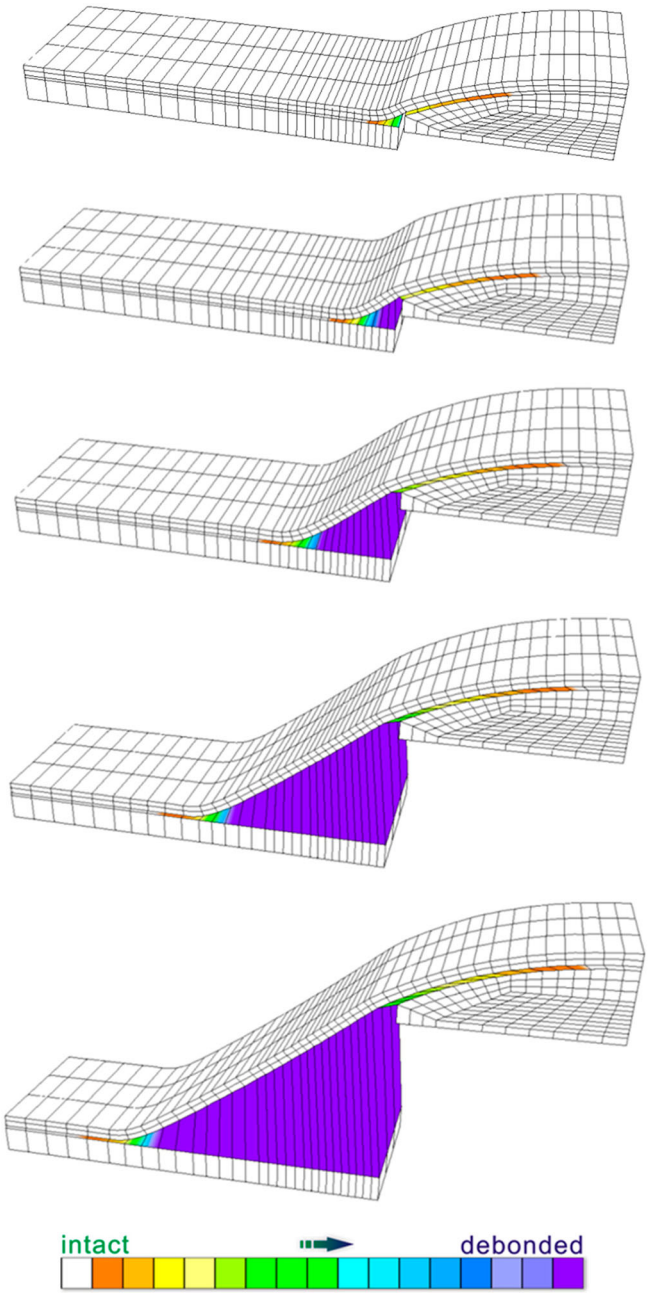

Figure 20. Evaluation of damage at the interface, piston vertical displacement: 10, 20, 40, 60 and 80 mm.

3.3.1 FE simulations of MAT test on steel/A1 specimen

The MAT tests were carried out at three temperatures: −5°C, 5° C and 10°C (Tzimiris 2017). By means of the methodology described in the previous Section, G and δ_C values were determined. In this thesis, for the sake of simplification, only the numerical simulations of MAT test at 10°C are presented. After a set of iterative simulations for MAT tests of Steel/A1 specimens, the input parameters of G=1.25 N/mm and δ_C = 2.1 mm are determined for the adhesive contact interface model. The elasticity parameters of the steel plate are E = 210 GPa and ν = 0.2. The Zener model parameters for modelling of the visco-elastic properties of membrane A1 are shown in (Li 2015). A linear increasing displacement controlled load with a loading speed of 5 mm/s is applied on the piston.

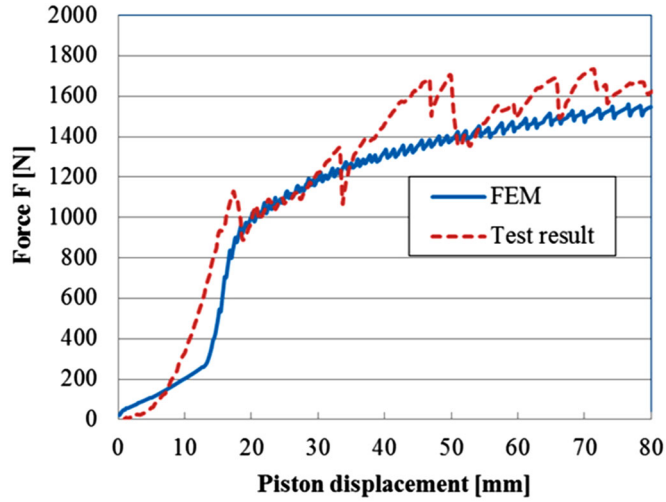

Figure 21. Comparison of modelling and test results for force-height relationship.

The in time distribution of horizontal stresses (σ_{xx}) in the membrane and the corresponding membrane deformed profiles are shown in Figure 18. High tensile and compressive strains were observed at the debonding tip area. The highest tensile strain occurred in the middle of the membrane, right above the piston. The debonding propagation and membrane deformations are similar with the laboratory observed ones.

The in time distribution of vertical stresses (σ_{yy}) in the membrane and the corresponding membrane deformed profiles are shown in Figure 19. High strain concentration was observed at the debonding tip area. The highest strain in membrane occurred at the free-stretching part which was completely debonded from the substrate plate. There is no stress/strain contour plot at the adhesive interface layer, however, a clear adhesive zone is shown by a tensile vertical strain area at the substrate plate.

The evaluation of the in time damage distribution at the interface and the corresponding membrane deformed profiles are shown in Figure 20. From this set of contour plots, the cohesive zone at the debonding tip area can be seen. Higher damage occurs at the debonded membrane interface area.

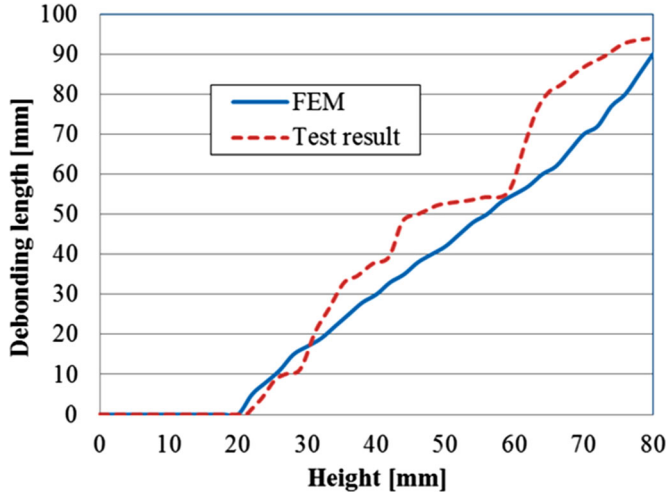

Figure 22. Comparison of simulation and test results for debonding length vs. height relationship.

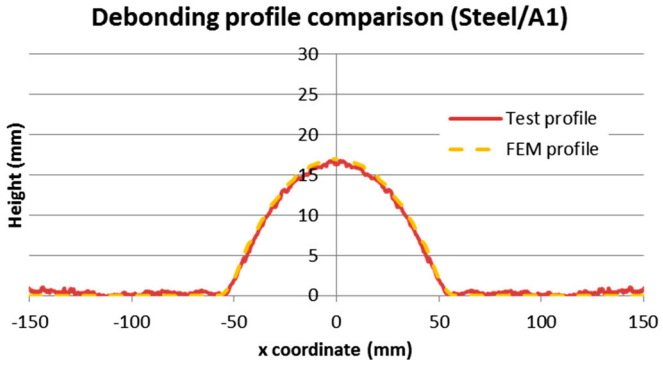

Figure 23. Debonding profile comparison between experimental and FEM results.

Slight damage occurs also between the piston and the membrane due to sliding deformation.

Figure 21 shows the comparison of the numerical prediction with the experimental results in terms of load–displacement curve. Since only a quarter of the MAT setup is simulated, the numerical result is magnified by a factor four times in order to compare with the test results.

It can be observed that the numerical predictions show good agreement to the experimental results. The load–displacement curve could be divided into three distinct stages: (1) pre-opening stage, (2) opening stage and (3) delamination stage. At the pre-opening stage, strain energy is accumulating at the bonding interface. At the opening stage, as the piston moved up to 20 mm, a clear kink point appears in the curve. After that, debonding at the interface between the membrane and steel plate is initiated and propagated constantly through the whole interfacial zone. It can also observed that, due to the inhomogeneity of the adhesive interface layer, the test curve shows severe force fluctuation during the membrane debonding. The small wiggles on the numerical result can be smoothed by reducing the contact interface element size in the numerical simulations.

The comparison of the membrane debonding length versus piston vertical displacement of Steel/A1 interface is given in Figure 22. It can be seen that the numerical predictions of the membrane debonding initiation and the speed of the debonding area propagation show good agreement with the experimental results.

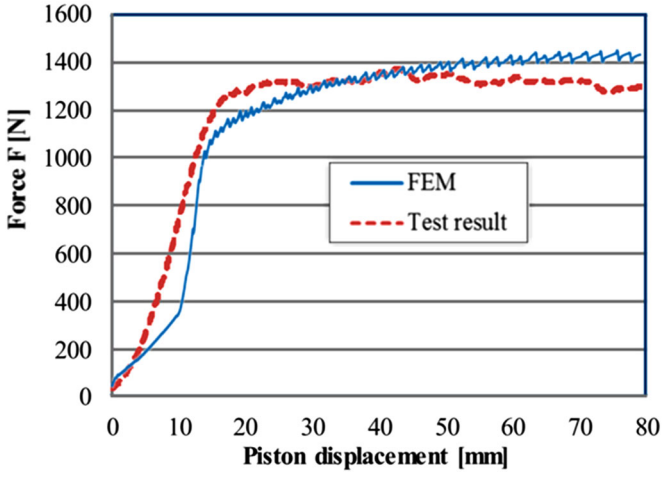

Figure 24. Comparison of modelling and test results for force-height relationship.

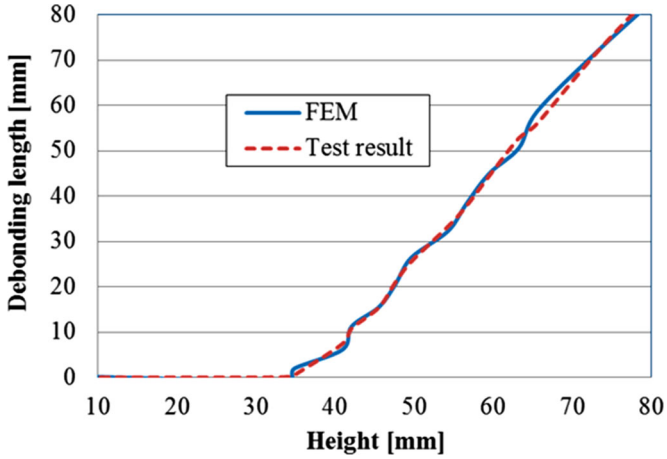

Figure 25 . Comparison of simulation and test results for debonding length vs. height relationship.

A membrane deformed profile comparison at the moment of debonding initiation is given in Figure 23. It shows that the numerically generated membrane deformed profile matches very well with the actual observed behaviour. It is further proved that the adhesive contact interface model is capable of describing the membrane bonding response.

3.3.2 FE simulations of MAT test on A1/Guss asphalt specimen

After a set of iterative simulations for MAT tests of A1/Guss asphalt specimens, the input parameters of $G = 2.12$ N/mm and $\delta_C = 2.6$ mm are utilised for the adhesive contact interface model. The visco-elastic properties of Guss asphalt and membrane A1 are shown in (Li 2015) respectively.

Figure 24 shows the comparison of the numerical prediction with the experimental results in terms of load-displacement. The comparison of the membrane debonding length versus piston vertical displacement of the A1/Guss interface is given in Figure 25.

It can be observed that the numerical predictions show good agreement with the experimental results. In contrast to the Steel/A1 specimen described in the previous section, this specimen shows quite steady response. The magnitude of the measured reaction force from the piston keeps constant during the

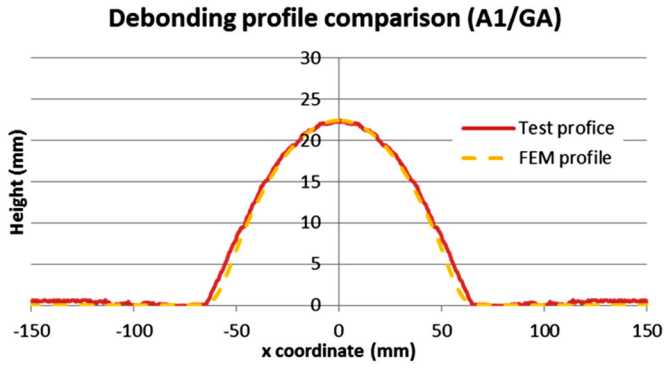

Figure 26. Debonding profile comparison between experimental and FEM results.

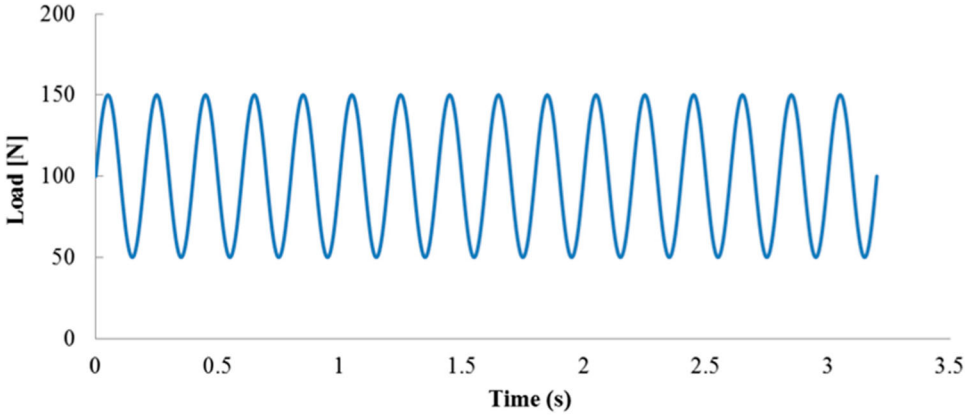

Figure 27. Load scheme of MAT cyclic tests.

membrane debonding area propagation and no force fluctuation occurs. Apparently, due to the characteristics of the Guss asphalt substrate, there is a uniform adhesive interface layer in this specimen to bond the membrane to the Guss asphalt substrate.

A membrane deformed profile comparison at the moment of debonding initiation is given in Figure 26. It shows that the numerical generated membrane deformed profile matches very well with the actual observed behaviour. This indicates that the adhesive contact interface model is capable of describing the membrane bonding response.

3.3.3 Modelling of MAT cyclic tests

The monotonic MAT tests provide a fundamentally sound, mechanistic methodology for the expedient ranking of the bonding characteristics of membrane products. The MAT device is also capable of investigating the fatigue response of membrane products under cyclic loading conditions at different temperatures. In our test programme, the membrane fatigue tests were performed at two temperatures ranges (10°C and 30°C). The fatigue tests at 10°C, were performed with a sinusoidal loading F ranging between $F_{\min} = 50\ N$and $F_{\max} = 150$ N at a frequency of 5 Hz. In this section, the modelling of MAT cyclic tests at 10°C is presented.

The loading scheme of MAT cyclic tests is shown in Figure 27.

The interface properties selected for this modelling are as follows: $G = 4.0$ N/mm, $\delta_C = 1.5$ mm, $\Delta_{max} = 8$ mm, $c = 0.2$, $\xi_0 = 1.0$, $k_1 = 30$, $\delta_0 = 1$ mm and $\delta_{\max} = 5$ mm. This set of parameters does not explicitly stand for any interface layer involved in our test scheme; instead, those damage parameters were intentionally chosen to demonstrate the capability of the contact interface element to model the fatigue response of membrane product in MAT test.

The accumulated damage in the interface layer between the membrane and the steel substrate as well as the steel piston, after 400 cycles of the load, depicted in Figure 27, is shown in Figure 28. The interface damage increases after each load cycle as expected. As the damage develops, the piston displacement also increases under the load. The higher damage occurs at the debonded membrane interface area and slight damage occurs also between the piston and the membrane due to sliding deformation.

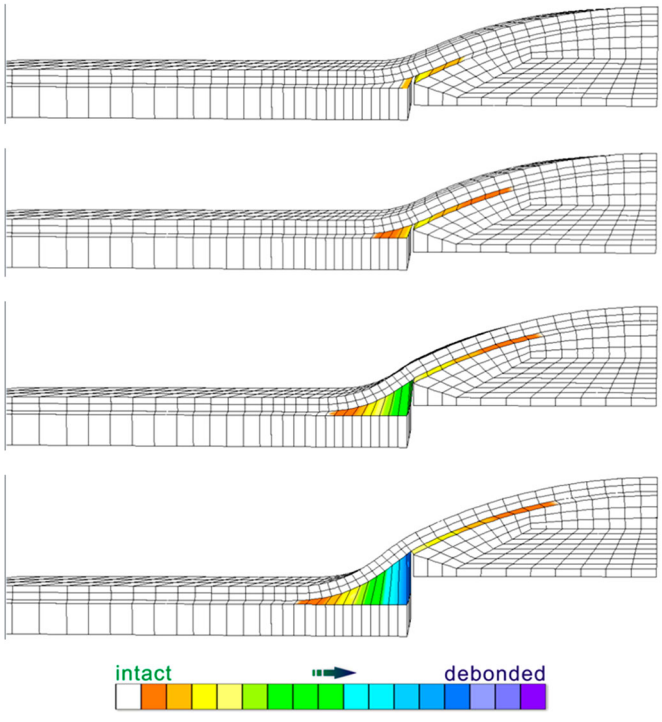

Figure 28. Evolution of damage accumulated at the interface layer.

4. Conclusions

In this contribution, the following main findings and remarks can be drawn:

- The MAT setup is capable of characterising the adhesive bonding strength of the various membranes with the surrounding materials.
- MAT results allow a better understanding of the performance of the membrane on the bridge structure allowing therefore optimisation of maintenance activities;
- The mechanical response of a membrane product is influenced not only by the surrounding substrate but also by environment temperatures;

- Critical energy release rate G is a fundamental physical quantity that can be utilised to quantify the membrane adhesive bonding strength with different substrates;
- The FE simulations show that the strain energy release rate can be indeed chosen as the physical parameter to quantify the membrane bonding characteristics.
- The adhesive traction separation law that is embedded in the contact interface element is capable to model the opening process of the bonding interface of the various membranes with the substrates. The numerical results indicate that, once the appropriate material parameters are available, the model shows good comparison with the observed behaviour in the MAT tests.

Acknowledgment

This work is part of the research programme of InfraQuest. InfraQuest is a collaboration between Rijkswaterstaat, TNO and the Delft University of Technology. This research project is funded by the Dutch Ministry of Transport, Public Works and Water Management (RWS). Their financial support is highly appreciated.

Disclosure statement

No potential conflict of interest was reported by the author(s).

References

Dannenberg, H, 1958. Measurement of adhesion by a blister method. *Journal of Applied Polymer Science*, 33, 509–510.

Gent, A., & Lewandowski, L. (1987). Blow-off pressures for adhering layers. Journal of Applied Polymer Science, 33, 1567–1577.

Li, J. (2015). Optimum design of multilayer asphalt surfacing systems for orthotropic steel deck bridges. PhD thesis. *Delft University of Technology*, Netherlands.

Liao, K., and Wan, K. T, 2001. Evaluation of film-substrate interface durability using a shaft-loaded blister test. *Journal of Composites Technology and Research*, 23, 15–20.

Liu, X., *et al.*, 2013. Test method to assess bonding characteristics of membrane layers in wearing course on orthotropic steel bridge decks. *Transportation Research Record*, 2360, 77–83.

Liu, X., et al., 2019. Modelling of membrane bonding response: part 1 development of an adhesive contact interface element. *International Journal of Pavement Engineering*.

Russell, H.G. (2012). Waterproofing membranes for concrete bridge decks. NCHRP Synthesis 425.

Tzimiris, G. (2017). *Experimental investigation of membrane materials used in multilayer surfacing systems for orthotropic steel deck bridges*. (PhD thesis). *Delft University of Technology*, Netherlands.

Williams, M. L, 1969. The continuum interpretation for fracture and adhesion. *Journal of Applied Polymer Science*, 13, 1.

Xu, X. J., Shearwood, C., and Liao, K, 2003. A shaft-loaded blister test for elastic response and delamination behavior of thin film-substrate system. *Thin Solid Films*, 424, 115–119.